Gone Shaftless

Mikhail D. Freeman

Mervin A. Marshall

Freeman and Marshall describe simulated model test results for the design of a shaftless thruster based on three symmetrical blades attached to an outer cylindrical casing.

Who should read this paper?

Anyone who has ever had a line wrapped around a propeller shaft, struck bottom in shallow water or experienced the limited manoeuvrability inherent in conventional marine propulsion systems will be interested in the work reported here. The findings show particular promise for the aquaculture industry, where close quarter operation among cages and mooring lines is an everyday reality.

Why is it important?

Shaftless thrusters are relatively new to the marine industry and offer significant potential benefits when compared with conventional propulsion systems. In particular, conventional systems (shaft driven propellers) are prone to debris tangling (e.g., fishing nets) and cavitation, which can pose safety hazards to both ship and crew due to potential loss of power.

The authors have designed and analyzed a shaftless propeller in which the roots of the blades are attached to an outer cylinder and point inward towards each other. Each blade is symmetrical and generates equal thrust in both directions of rotation, forward and reverse.

Numerical simulations were used to evaluate the structural integrity, flow trajectories and thrust characteristics of the model thruster. These simulations were used to illustrate the potential performance of the shaftless thruster relative to a conventional propeller. Results reveal a low pressure / high velocity area in the centre of the shaftless thruster that would give free passage of any potential debris that might otherwise lead to fouling of a conventional propeller. Furthermore, the authors suggest that further analysis is needed to determine optimal blade design and to minimize any tendency towards cavitation.

About the authors

Mikhail D. Freeman is a graduate student at the Fisheries and Marine Institute of Memorial University. His background is in marine engineering and he is currently completing a Master of Technology Management, focusing on engineering and applied science. Dr. Mervin A. Marshall is a faculty member at the Fisheries and Marine Institute. His area of expertise is in structural integrity monitoring using random vibration approaches.

AN ANALYTICAL INVESTIGATION INTO THE DESIGN OF A SHAFTLESS THRUSTER USING FINITE ELEMENT AND COMPUTATIONAL FLUID DYNAMICS APPROACHES

Mikhail D. Freeman and Mervin A. Marshall
School of Maritime Studies, Fisheries and Marine Institute of Memorial University of Newfoundland, St. John's, Newfoundland and Labrador, Canada

ABSTRACT

Traditional marine propellers and thrusters driven by a shaft are associated with problems such as debris tangling (e.g., fishing nets), cavitation and limited machinery arrangement. The elimination of such impediments is being investigated through an alternative propulsion method, which is shaftless. To achieve this objective, a model was designed and analyzed using FEA (finite element analysis) and CFD (computational fluid dynamics). By applying these analytical procedures, it was possible to simulate the propeller region under various rotating conditions, so that detailed information on the energy transfer of the inherent complex, unsteady flow field could be obtained. Usually, the design of such structures is enhanced through actual experimental simulations in the appropriate facilities. However, because experimental tests in such facilities (e.g., towing tanks and cavitation tunnels) are sometimes very time-consuming and exorbitant, it is always beneficial to carry out analytical simulations prior to actual testing, so a better understanding of the structure and the results obtained experimentally can be achieved. (Moreover, this approach could also reduce the time and cost associated with such experiments.) In this paper, the analytical simulations approach is being adopted.

Based upon the reported results and evaluations, it was concluded that a shaftless thruster of suitable efficiency (in the marine industry) could effectively eliminate tangling, and the need for a conventional driving shaft.

KEY WORDS

Shaftless thrusters; Finite element analysis; von Mises Failure Criteria; Free vibration; Computational fluid dynamics; Pressure-velocity distribution; Bernoulli Effect; Cavitation

NOMENCLATURE

A	=	outlet area	σ_y	=	yield stress of the material
BPF	=	blade passing frequency	$\sigma_1, \sigma_2, \sigma_3$	=	principle stresses on principle planes 1, 2 and 3, respectively
F	=	force			
f_n	=	natural frequency	T	=	thrust
f_r	=	resonant frequency	V	=	flow velocity
m	=	fluid mass	ζ_n	=	modal damping ratio
p_1, p_2	=	hydrostatic pressure at the inlet and outlet, respectively			

INTRODUCTION

Thrusters driven by a shaft are sometimes not practical for vessel manoeuvrability (particularly in shallow waters) because of tangling and damage attributable to debris – e.g., fishing nets, and cables. When floating debris comes in contact with propellers, damage can occur in the edge region of the blades. Such damage may lead to cavitation, fouling, and premature propeller failure, if not repaired [Carlton, 2007]. Furthermore, when debris tangles the propeller shaft, a ship could lose its propulsion and manoeuvrability, which could pose a great safety hazard to the ship and its crew. A shaftless propulsion system would decrease tangling and, consequently, reduce the associated problems [Brunvoll, 2005].

Computational fluid dynamics (CFD) is an efficient analytical tool to study fluid-structure interaction. Using this type of analysis, it is possible to analyze and modify models prior to testing and prototyping. The finite element analysis (FEA) is a popular numerical technique for finding approximate solutions of partial differential equations and integral equations for fluids and structural analysis of mechanical systems. FEA software provides a wide range of simulation options for controlling the complexity of both modelling and analysis of a system. In this paper, the FEA and CFD approaches are being used to design and analyze the shaftless propulsion system, which is being proposed. To achieve this purpose, the following approach has been taken:

- a geometrical design of the propeller blade;
- structural integrity analysis of the rotating region;
- dynamic analysis to assess natural frequency of the system;
- thrust analyses at various propulsion speeds;
- pressure and velocity vector distribution analysis in the rotating region; and
- a blade pressure and velocity reaction analysis.

DESIGN

Overall Geometry

The design of the proposed shaftless thruster is original, and was designed and modelled using SolidWorks™. (This allowed the model to be changed parametrically.) The propeller tunnel diameter tested was based on the commercially available Vetus™ Bow Thruster dimensions to compare the thrust generated. Figures 1 and 2

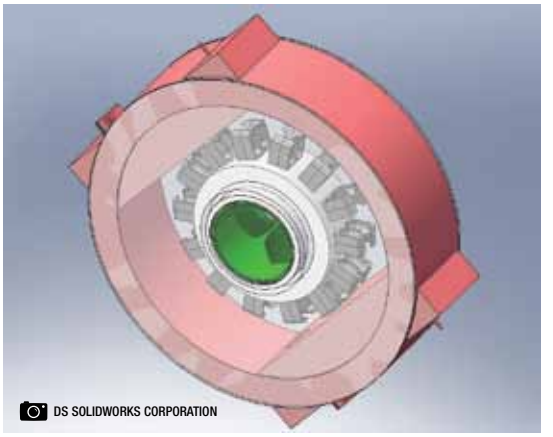

Figure 1: Trimetric assembly.

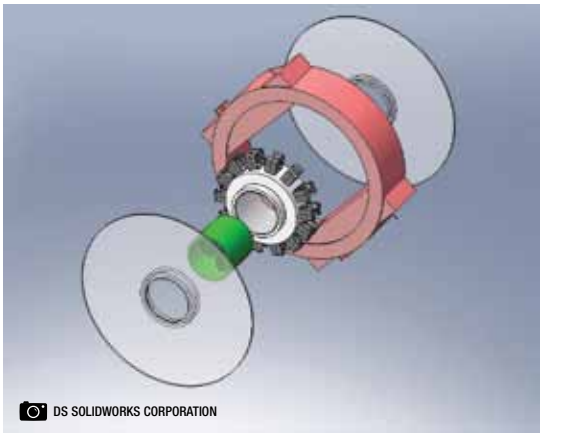

Figure 2: Trimetric exploded assembly.

show the geometrical design of the thruster being investigated. [Details of how the shaftless thruster is driven are not described or shown in this paper.]

Propeller Blade Geometry

In conventional shaft-driven propellers, a pressure difference is produced between the forward and rear surfaces of a marine propeller blade, which is in the form of a helical screw. The water is accelerated by the rear surface, known as the driving face. This screw is formed by a number of blades set at an angle to the plane of rotation, and are attached to the boss (i.e., hub) at the end of the driving shaft. There are many design theories for conventional propellers that include non-dimensional coefficients displayed in logarithmic propeller designs. The shaftless propeller blade differs vastly from a conventional marine propeller blade. In this paper, the proposed shaftless propeller was modelled, so that the roots of the blades are large and are attached to an outer casing to increase the driving face surface area. Each blade is symmetrical for use in the forward or reverse directions. The propeller and tunnel characteristics are presented in Table 1. Figures 3 to 6 illustrate the geometrical configuration of the blades.

	Formulae	Value
Disk Area, A, [m^2]	$\frac{\pi d_T^2}{4}(\text{tunnel}) - \frac{\pi d_V^2}{4}(\text{center void})$	0.060
Differential Radius [m]	D	0.240
Number of Blades	N	3.000
Blade Thickness Ratio	$\frac{t}{2D}$	0.042
Pitch, P, [m]	$2\pi r\tan\theta$	0.123
Pitch Angle [degrees]	θ	56.86
Pitch Ratio	$\frac{P}{2D}$	0.256
Surface Area (per side per blade) [m^2]	A_s	0.030

Table 1: Property geometry parameters.

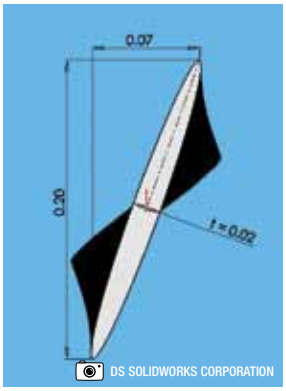

Figure 3: Propeller root geometry.

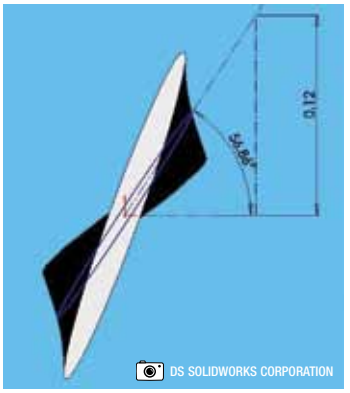

Figure 4: Propeller pitch.

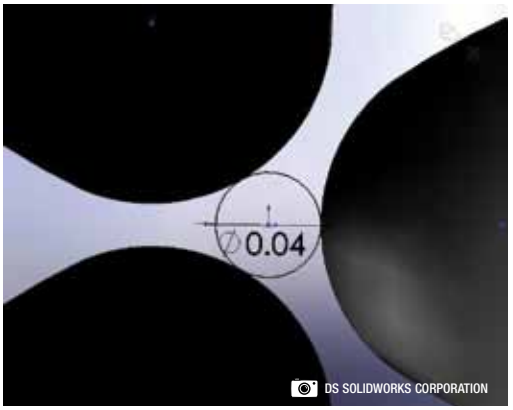

Figure 5: Centre void diameter.

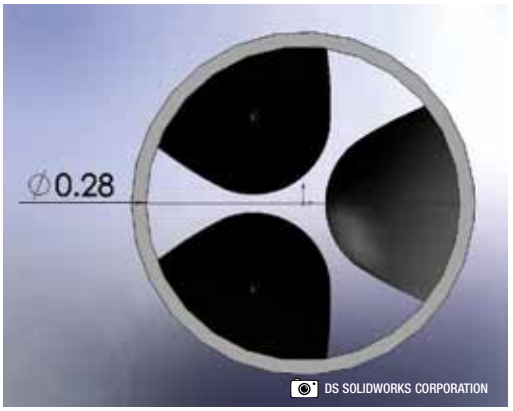

Figure 6: Tunnel diameter.

ANALYTICAL INVESTIGATION

In this section, the analytical simulations are presented. The CFD simulations were carried out using Cosmos FloWorks™ – an integrated component in SolidWorks™. These analytical computations were conducted within the propeller speed range of 1000 to 5500 rpm, inclusive, at increments of 500 rpm. All structural analyses (stress and frequency domain) were carried out using Cosmos Works™.

Structural Integrity – Rotating Region

The material used for the propeller blades is Aluminum 2018. For ductile materials, such as aluminum, if the magnitude of the external forces is substantial, the material undergoes plastic deformation, if the induced stresses (attributable to the applied loads) exceed the yield stress of the material. (In this case, there are permanent changes in atomic positions of the structural material.) Several theories such as Tresca and von Mises propose different failure criteria. Notwithstanding, for ductile materials, the von Mises theory is more widely used, because it is more conservative in the estimation of failure [Spyrakos, 1996]. Therefore, in this paper, the von Mises theory is used.

According to von Mises, the material yields (i.e., experiences plastic deformation) when the principal stresses (caused by the externally applied loads) at a point or region in the structure satisfy the following relationship:

$$\sigma_y = \sqrt{0.5\left[(\sigma_1-\sigma_2)^2+(\sigma_2-\sigma_3)^2+(\sigma_3-\sigma_1)^2\right]}. \quad (1)$$

As a result, direct comparison of the von Mises stress with the yield stress, σ_y, allows identification of the regions that have yielded.

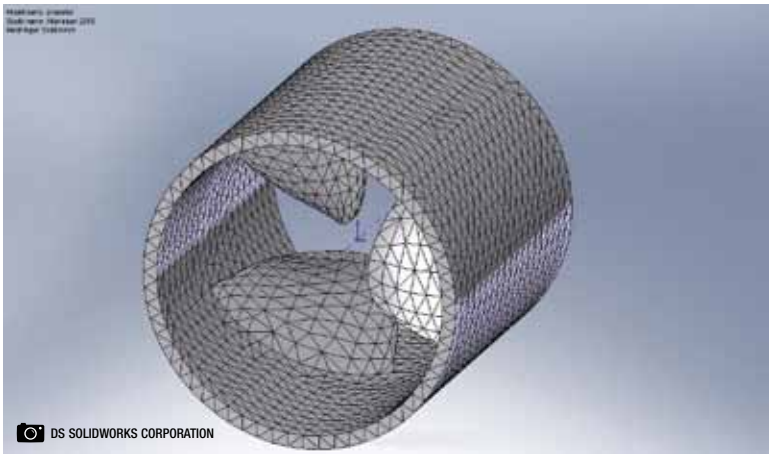

Figure 7: FEA discretization of the rotating region of the propeller.

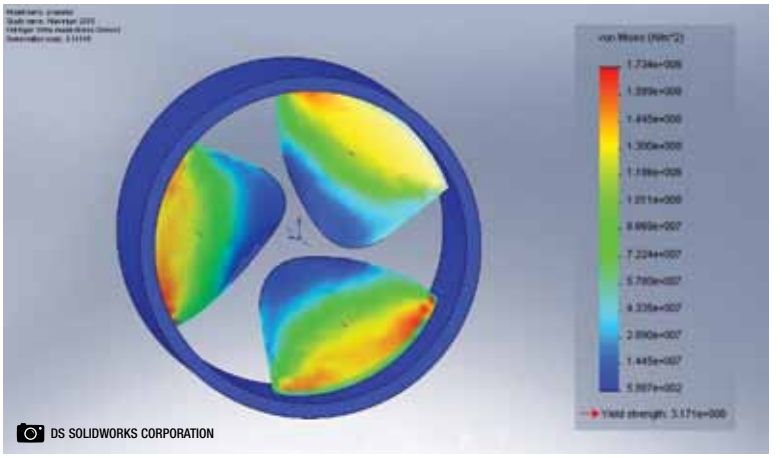

Figure 8: von Mises stress distribution at a speed of 5500 rpm.

Before the detailed stress analyses were carried out on the propeller region, the structure was first discretized (i.e., meshed) as illustrated in Figure 7. The largest torque was achieved when the propeller was tested at 5500 rpm. The resulting stress distribution at that speed is shown in Figure 8. Observe that all the stresses on the blade are less than the yield stress of the material (i.e., Aluminum 2018), and seem to reaffirm that the von Mises failure criterion has been satisfied, as alluded to earlier. Accordingly, one would not expect material failure, attributable to yielding, when the propeller is operating at a speed which induces the maximum torque of 819.61 Nm. [All loads used in the analyses (such as the maximum torque of 819.61 Nm) were determined from the flow analyses, which incorporated the hydrodynamic loads.]

Natural Frequency and Mode Shape Analyses

Excessive vibrations can adversely affect the operation of mechanical systems and are related to the resonant frequency of vibration of the system. If one frequency of a harmonic excitation (or angular velocity) coincides with one of the resonant frequencies of the system, the amplitude of vibration of the system may become very large. Such a condition is referred to as resonance. It is always desirable to avoid or at least design for resonance. The natural frequencies are dynamic characteristics of the

Mode Number	Frequency, f_n, Hz		Frequency, f_n, rpm		Propeller Speed	
	In Air	In Water	In Air	In Water	BPF, Hz	rpm
1	342.77	319.77	20566.20	19186.20	50	1000
2	342.79	319.84	20567.40	19190.40	75	1500
3	343.41	320.47	20604.60	19228.20	100	2000
4	1946.10	1819.20	116766.00	109152.00	125	2500
5	1947.60	1819.70	116856.00	109182.00	150	3000
6	1947.70	1820.70	116862.00	109242.00	175	3500
7	2092.10	1960.40	125526.00	117624.00	200	4000
8	2093.20	1961.40	125592.00	117684.00	225	4500
9	2096.10	1963.80	125766.00	117828.00	250	5000
10	3475.90	3271.80	208554.00	196308.00	275	5500

Table 2: Natural and operating frequencies of the shaftless propeller.

system specified by its stiffness and inertial properties. For most metals, the inherent material modal damping ratio, ζ_n, is less than 5%; therefore, the resonant frequency, f_r, will be approximately equal the natural frequency, f_n, of the system. (N.B.: $f_r = f_n\sqrt{1-\zeta_n^2}$.) (Natural frequencies and mode shape analyses were calculated using the subspace iteration technique, which is available in Cosmos Works™.)

Table 2 shows the computed natural frequencies for the first 10 modes of vibration. An examination of the results presented suggests that since the possible operating speeds of the propeller are significantly lower than the natural frequencies of the system, the propeller would not experience resonance; that is, excessive displacements attributable to vibrations.

To better understand the dynamic behaviour of the propeller at the various modes of vibration, dynamic mode shape (i.e., eigenvectors) were computed. Figures 9 to 12 show typical mode shapes for the first four modes of vibration. [Mode shapes are eigenvectors, and do suggest relative displacement as opposed to actual displacements.]

CFD Simulations – Flow Trajectories

To investigate the fluid-structure-interaction, an external computational domain for the flow simulation was created in Cosmos FloWorks™. This domain is approximately 4 m from the model in all axes, and is a rectangular parallelepiped. (Ambient pressure and temperature were the conditions in all simulations.) The FEA mesh of this critical region is depicted in Figure 13. Typical flow trajectories (within this boundary region) are illustrated in Figures 14 to 17. Note that these flow trajectories display a visual image of the fluid flow distribution at the inlet and outlet of the propeller. Moreover, the fluid velocity

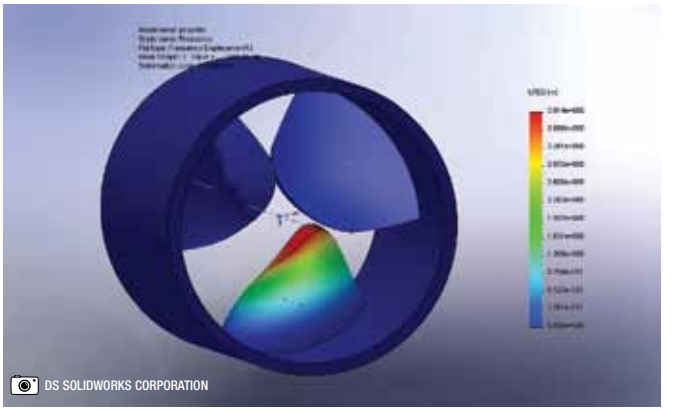

Figure 9: Mode shape 1 – frequency 342.77 Hz.

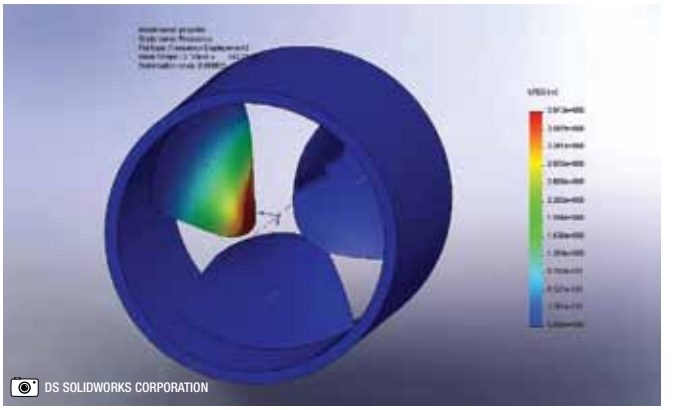

Figure 10: Mode shape 2 – frequency 342.79 Hz.

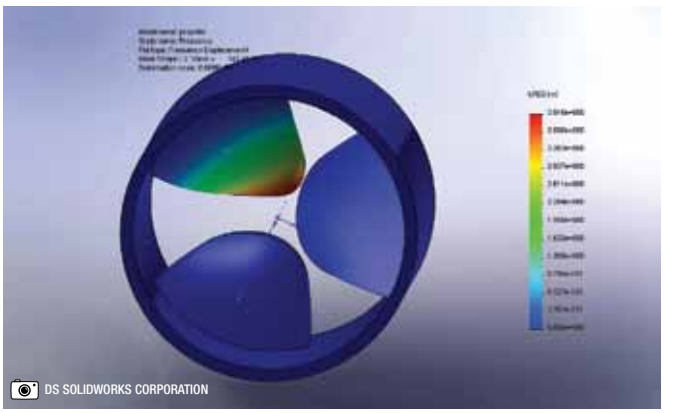

Figure 11: Mode shape 3 – frequency 343.41 Hz.

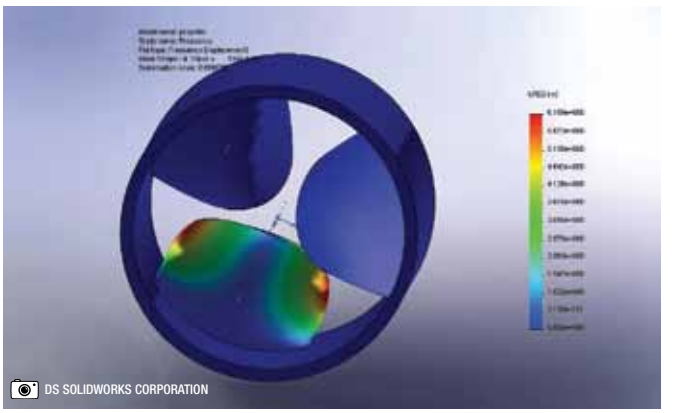

Figure 12: Mode shape 4 – frequency 1946.1 Hz.

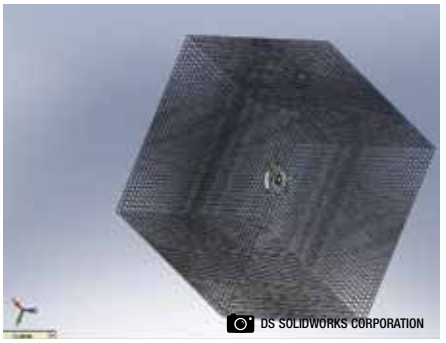

Figure 13: Discretization of the critical boundary region used for CFD analyses.

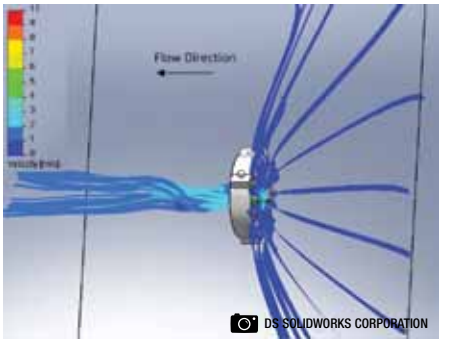

Figure 14: Flow trajectory from the propeller rotating at 1,000 rpm.

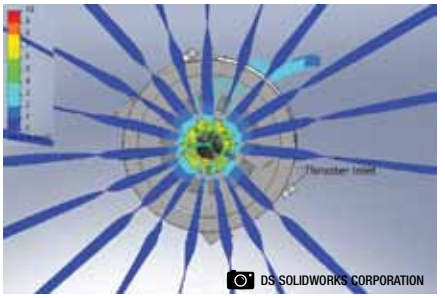

Figure 15: Flow trajectory from the propeller rotating at 2,000 rpm.

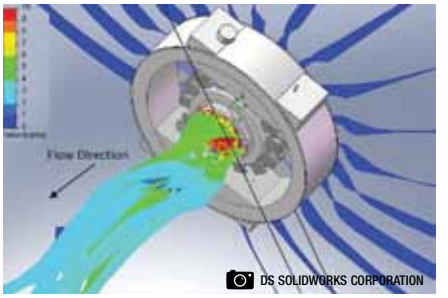

Figure 16: Flow trajectory from the propeller rotating at 1,000 rpm.

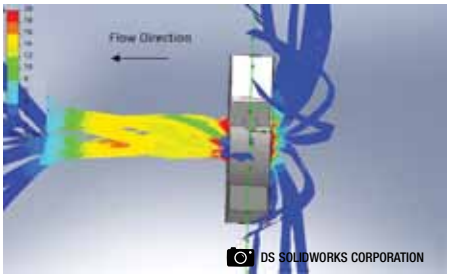

Figure 17: Flow trajectory from the propeller rotating at 5,500 rpm.

variation can be seen in the flow concentrations. An advantage of these visual flow images is to facilitate in the refinement when designing models (i.e., when a decrease of turbulence around solids is required) by noting where high or low pressures and velocities may be problematic. This statement is exemplified by observing how the flow trajectories illustrated in Figures 14 to 17 depict the fluid velocity distribution from the dispersed suction at the inlet (i.e., to the right of the propeller) to the concentrated flow at the outlet – to the left of the propeller.

Thrust Analyses

The thrust exerted by the propeller was computed by regarding the propeller as a reaction machine. [It should be emphasized that, although the thrust is calculated in ideal conditions, an *open-water* test should be carried out to calculate working capacities based on boat hull resistance and speed of advance. When the speed of advance is zero, this creates a special operating condition. This condition is important when considering the design of tugs and other similar crafts (e.g., fishing trawlers). Generally, these vessels are expected to spend an important part of their service duty at zero ship speed (i.e., bollard pull) and, at the same time, develop

full power [Carlton, 2007].] (This was also done for comparison with the published data of the Vetus™ Bow thruster shown in Table 3.) Consequently, the thrust generated from the shaftless propeller was calculated using the rate of change in momentum from the inlet to the outlet by applying Newton's second law of motion. The mass flow rate and velocity were found at the inlet and outlet faces of the rotating tunnel of the propeller. In mathematical terms, the force relationship from the mass flow rate and velocity can be represented as:

$$F = T = \frac{dm}{dt}V_2 - \frac{dm}{dt}V_1 + (p_2 - p_1)A_2 \ . \qquad (2)$$

However, since the hydrostatic pressures at the inlet and outlet are the same (i.e., $p_{1=}p_2$), the above expression may be rewritten as:

$$F = T = \frac{dm}{dt}V_2 - \frac{dm}{dt}V_1 \ . \qquad (3)$$

Here, subscripts 1 and 2 refer to the inlet and outlet, respectively.

A graph of thrust versus propeller speed is shown in Figure 18. A perusal of this graph clearly suggests that as the speed (rpm) increases, so does the thrust. It should be noted that although the thrust is increasing, at high speeds, a low pressure is created at the inlet to the propeller. If this pressure falls to the vapour pressure of the fluid, cavitation will occur. When cavitation occurs on ship propellers, there will be, beyond certain critical revolutions, a progressive break-down in the flow and consequent loss of thrust [Carlton, 2007]. As illustrated in Figure 19, low pressures occur at the inlet at the high speeds. This is why the propeller was only tested at 5500 rpm, which is common for conventional propellers of this diameter (i.e., 150-300 mm). For instance, the commercially available Vetus™ Bow thrusters (an example of which is illustrated in Figure 20) publicizes similar thrusts for the respective tunnel diameter. (Refer to Table 3.)

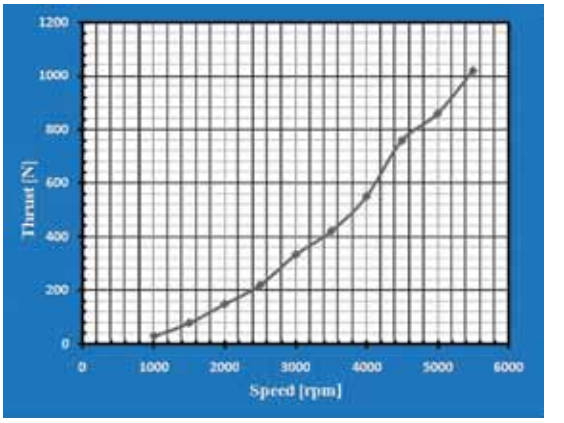

Figure 18: Thrust vs. speed.

Technical Data	BOW75	BOW95	BOW125	Shaftless
Thrust [N]	800 – 12 v 850 – 24 v	950 – 12 v 1050 – 24 v	1250 – 12 v 1400 – 24 v	1020†
Power [kW] (hp)	4.4 (6)	5.8 (8)	5.7 (8)	
Motor, Reversible d.c.	yes	yes	yes	
Tunnel Diameter [mm]	185	185	250	279
Weight excld. Tunnel [kg]	26	30	37	

†This is the thrust at a speed of 5500 rpm.

Table 3: Vetus™ BOW125 specification displaying similar thrust values.

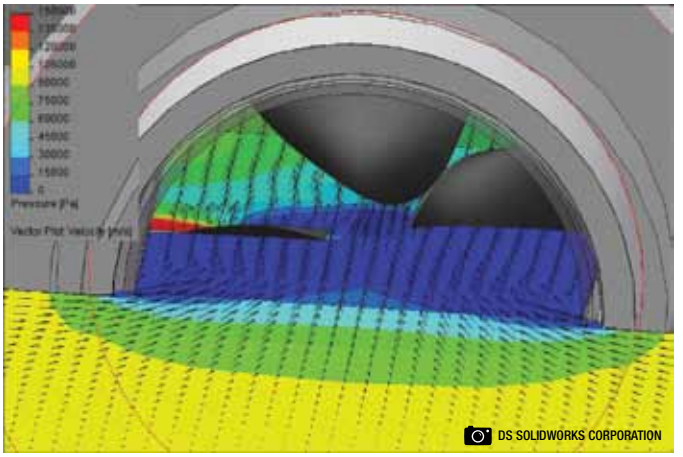

Figure 19 : 5500 rpm inlet pressure-vector distribution.

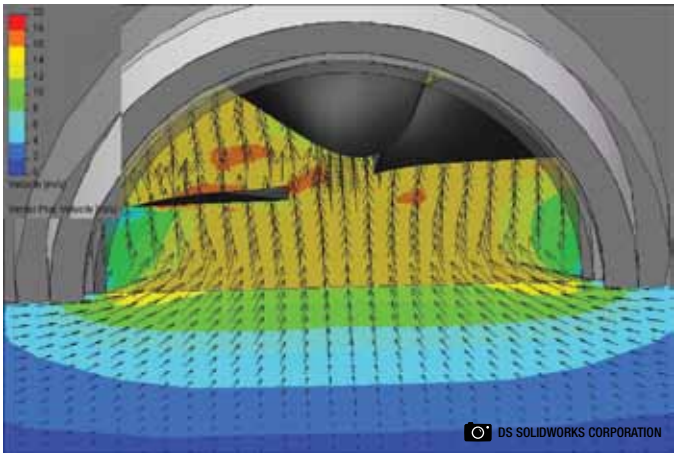

Figure 21: 3000 rpm inlet velocity-vector distribution.

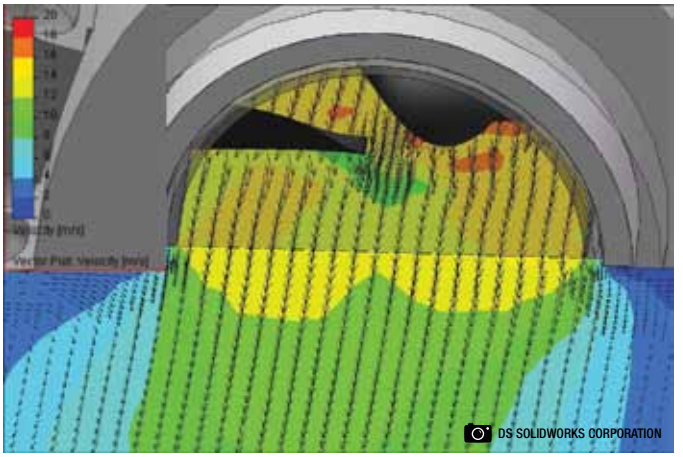

Figure 22: 3000 rpm outlet velocity-vector distribution.

Figure 20: Vetus™ Bow Thruster – Model BOW125 [Vetus, 2009].

Velocity-Vector Simulations

An important feature of the shaftless thruster is the way it distributes the fluid in the rotating region. The geometrical pattern of the propeller causes the fluid to be concentrated (at the highest velocity) in the centre void at both the inlet and the outlet. It is this unique characteristic of the shaftless propeller that causes debris to be forced into the centre void and, potentially, avoid any tangling and decrease propeller interference. Examples of this phenomena were shown earlier in Figure 17, and subsequently in Figures 21 and 22 by observing the concentration of the flow stream, which represents high velocity flow (symbolized by the vectors) in the centre void region at both the inlet and outlet of the rotation region.

Pressure-Vector Simulations

To understand the behaviour of the propeller better, pressure-velocity

simulations were carried out. An examination of some typical results depicted in Figure 23 and Figure 24 clearly illustrates the *Bernoulli Effect*; that is, the lowering of pressure in regions where the velocity flows is increased. (The net effect result is low pressures at the centre void and high pressures at the blade roots of the propeller.) This resulting pressure distribution further exemplifies why the passing of debris through the centre void is facilitated in the region where velocity vectors are concentrated.

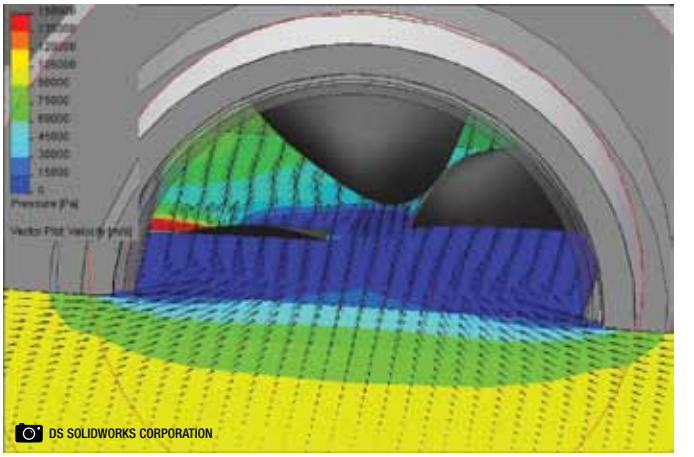

Figure 23: 3000 rpm inlet pressure-vector distribution.

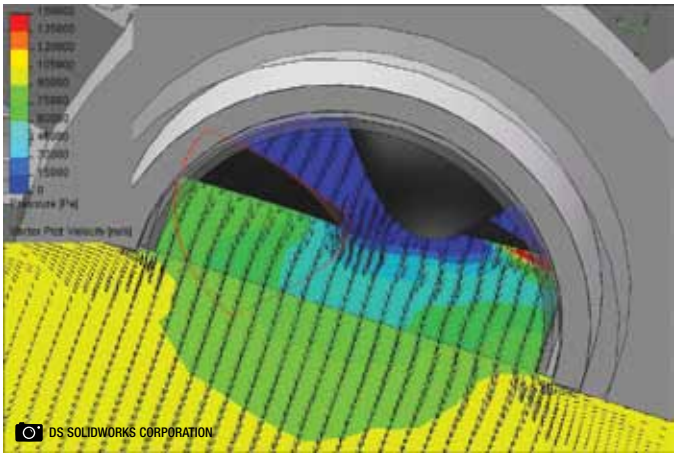

Figure 24: 3000 rpm outlet pressure-vector distribution.

Blade Surface Pressure and Velocity-Vector Simulations

Analyses were carried out to assess the velocity and pressure distribution on the surfaces of the propeller blades to assess their influence on thrust. Typical results from these analyses are portrayed in Figures 25 to 28. In Figures 25 and 27, it can be seen that most of the velocity is generated at the root of the propeller blade. This would, therefore, insinuate that by increasing the surface area or the number of propeller blades, the propeller could potentially generate more thrust.

Moreover, the pressure-vector distributions (shown in Figures 26 and 28) offer insight into potential cavitation areas. As the speed of the propeller increases, so does the amount of low pressure areas across the blade. These are the potential cavitation areas. Therefore, by changing blade geometry, such as pitch angle, these low pressure regions could be reduced.

Earlier works on models (and at full scale) suggest that the back or suction side cavitation – of the type causing thrust breakdown – could be avoided by increasing the blade surface area [Carlton, 2007]. As a result, it is suggested that computational fluid dynamics simulations, including cavitation studies, be carried out using various blade geometries.

CONCLUDING REMARKS

It should be emphasized that the purpose of the analyses was not to imply a superior system. Rather, these analyses were used to

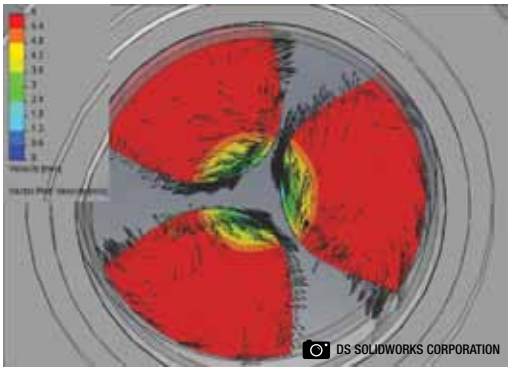

Figure 25: 3000 rpm blade surface velocity-vector distribution.

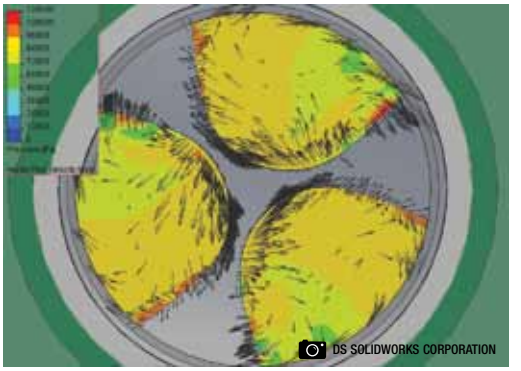

Figure 26: 3000 rpm blade surface pressure-vector distribution.

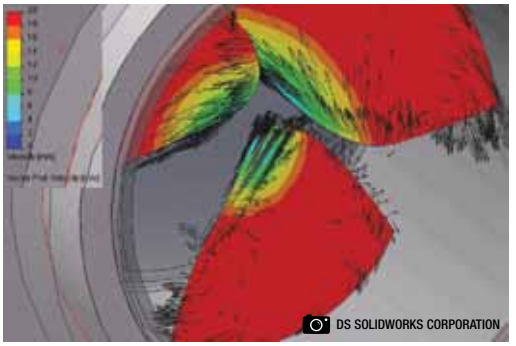

Figure 27: 5500 rpm blade surface velocity-vector distribution.

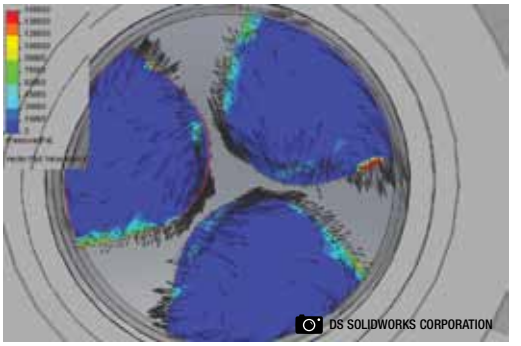

Figure 28: 5500 rpm blade surface pressure-vector distribution.

demonstrate the potential of a shaftless arrangement by presenting the areas of the system that could be beneficial for comparison with conventional arrangements. Based upon the reported results and evaluations, it can be concluded that a shaftless thruster, of suitable efficiency, could effectively eliminate tangling associated with propellers driven by a conventional shaft. A dynamic analysis using FEA approaches (i.e., von Mises stress and free vibration analysis) showed that Aluminum Alloy 2018 was a suitable material for the propeller and that operating speeds are attainable without excessive vibration and material failure attributable to yielding. The computational fluid dynamic analyses gave insight into the fluid-structure interaction. This resulted in flow trajectories which displayed visual images of the pressure and velocity distributions at the inlet and outlet of the propeller. (The low pressure and high velocity at the centre void region offers a free passage for debris associated with tangling.) Furthermore, the pressure and velocity distribution computations on each blade surface could be used to facilitate optimal blade design and decrease cavitation that could develop in the rotating region. From the mass flow rate computations, it was possible to compute the resulting thrust, by treating the propeller as a reaction machine.

RECOMMENDATIONS FOR FURTHER STUDY

From the experience gained in carrying out the research for this paper, the following is recommended:

1. A mechanical event simulation (dynamic analysis) should be carried out to integrate the driving mechanism with the shaftless thruster.

2. A scale model of the shaftless thruster should be constructed and tested in the appropriate facilities (e.g., wave tanks) to compare experimental results with the results obtained from the CFD and FEA approaches presented in this paper.

3. Computational fluid dynamics simulations, including cavitation studies, should be carried out using various blade geometries.

ACKNOWLEDGEMENTS

The authors would like to thank the Marine Institute and the Faculty of Engineering and Applied Science, Memorial University, Newfoundland and Labrador, for use of their facilities.

REFERENCES

Brunvoll, A.S. [2005]. *Brunvoll presents a "Rim driven thruster"* (RDT). Retrieved from http://www.brunvoll.no/public/cmsmm.nsf/lupgraphics/Brunvoll_developes_RDT.pdf/$file/Brunvoll_developes_RDT.pdf.

Carlton, J.S. [2007]. *Marine propellers and propulsion*, 2nd edition. London, England: Butterworth-Heinemann.

Spyrakos, C.C. [1996]. *Finite element modeling in engineering practice*. Pittsburgh, PA: Algor, Inc. Publishing Division.

Vetus. [2009]. *Vetus Catalogue 2009*. Retrieved from http://www.vetus.nl/en/index.php.

ADDITIONAL READING

Brunvoll, A.S. [2010]. *Rim driven thruster: a new thruster concept*. Retrieved from http://www.brunvoll.no/public/cmsmm.nsf/lupgraphics/RDT%20leaflet%2012-2009.pdf/$file/RDT%20leaflet%2012-2009.pdf.

Freeman, M.D. [2009]. *An analysis of a shaftless thruster design using finite element procedures*. Bachelor of Technology thesis, Memorial University of Newfoundland, St. John's, Newfoundland, Canada.

Hansen, S.L. [2006]. *Applied SolidWorks*. New York: Industrial Press.

Iannelli, J. [2006]. *Characteristics finite element methods in computational fluid dynamics*. Germany: Springer Berlin Heidelberg.

Johnson, S., Landay, W., McCoy, K., and McCullough, B. [2006, April 6]. *Integration of energy efficient propulsion systems for future U.S. navy vessels*. House Armed Services Committee.

Newman, J.N. [1977]. *Marine hydrodynamics*. Cambridge, Mass: MIT Press.

Ottosen, N. [1992]. *Introduction to the finite element method*. Great Britain: Prentice Hall International.

Raftoyiannis, J. and Spyrakos, C.C. [1997]. *Linear and nonlinear finite element modeling in engineering practice*. Pittsburgh, PA: Algor, Inc. Publishing Division.

